

Atom Probe Tomography and Transmission Electron Microscopy: A powerful combination to characterize the speciation and distribution of Cu in organic matter

Sarib Jadoon^{*1}, Michael Schindler¹, Mark G. Wirth², Odeta Qafoku², Libor Kovarik³,

Daniel E. Perea²

1. Department of Earth Sciences, University of Manitoba, Winnipeg, MB, Canada R3T 2N2
2. Environmental Molecular Sciences Laboratory (EMSL), Pacific Northwest National Laboratory, Richland, WA 99354, USA
3. Physical and Computational Sciences Directorate, Pacific Northwest National Laboratory, Richland, WA 99354, USA

**Corresponding author email: jadoons@myumanitoba.ca*

Supplementary Information

Background information on smelter-impacted soils and study area

The deposition of PM in mining impacted soils is a global concern. The deposition of metal(loid) bearing PM increases the concentration levels of metal(loid)s in the surficial layers of soils.¹ The weathering of PM is controlled by both soil environmental/matrix conditions and composition of PM and results in the release of metal(loid)s and their subsequent sequestration by solid and colloidal phases composed of OM and minerals.² Studies assessing the environmental fate of PM in mining/smelter impacted soils cannot always explain the observed moieties of

metal(loid) species in soils. In this regard, Lanteigne et al. ³ and Schindler et al. ⁴ showed that the higher mobility of Cu vs Ni in soils around the smelter complexes in Sudbury is a result of the higher solubility of Cu- versus Ni-mineral phases occurring in the micrometer-size fraction of the smelter emissions.

The area of this study extends around the city limits of Rouyn-Noranda, Quebec. It surrounds the Horne smelter, which is considered a critical emission source of PM contaminated with heavy metal(loid)s. The ore processed at the Horne smelter included minerals like sphalerite, pyrite, galena, pyrrhotite, chalcopyrite and magnetite, as well as native silver and gold ⁵ with pyrite, pyrrhotite, chalcopyrite and magnetite comprising up to 85% of the mass.⁶ PM emissions from the Horne smelter occurred for over a century.⁷ Since 1976, the smelter predominantly processes electronic waste containing metal(loid)s such as Cu.

Studies on the environmental impact of smelting activities in Rouyn Noranda focused on the concentrations and speciation of metal(loid)s in lakes, soils, rock coatings, snow samples and biota.⁸⁻¹³ Knight and Henderson ¹⁰ classified PM in the surficial soils surrounding the smelter based on size, texture and composition and showed that rounded and spherical smelter-derived PM are the most abundant type of PM. The rounded particles are further classified into tabular (Fe and Fe+Al+Si), plated (Fe), granular (Fe+Al+Si), etched (Cu+Fe+Si), and lunar (Na+Al+Si) textures, which mostly represent slag based dust released from Cu smelting operations over the course of time. The above authors proposed that this slag-based dust is very resistant to weathering and hardly contributes to the metal(loid) concentrations in humus, whereas the majority of Cu, Zn and Pb metal(loid) phases in humus represents weathered and alteration products of labile dust released from smelting operations.

Materials and methods

Sample preparation and Bulk Analytical Techniques

All collected samples were taken back to the lab in sealed plastic bags to a lab at Laurentian University (circa 4 hours' drive), sieved (< 1.4 mm), dried in an oven at 80°C for three days and stored under dry conditions for further examinations.

The pH value of the soil samples was measured by mixing 2 g of soil with 10 mL of a 0.01 M CaCl_2 solution¹⁴, The mixture was thoroughly stirred for 30 minutes and allowed to settle for 15 minutes before the pH measurement. Total carbon and sulfur of the samples were measured in the Ontario Geological Survey Geoscience Laboratories (Geo Labs) with a LECO CS844. This analysis was conducted by combustion of 0.2g of soil in a stream of purified O_2 gas and later passed over a heated catalyst, oxidizing total S and C to SO_2 and CO_2 , respectively, which are then detected by two non-dispersive infrared cells.¹⁵ The soil digestion process and inductively coupled plasma-mass spectrometry (ICP-MS) measurements of the soil fractions were conducted at the Geo Labs, Sudbury, ON, Canada. Samples were prepared in a reverse aqua-regia digest following the Burnham¹⁶ method and analyzed with an iCAP Q ICP-MS (Thermo Scientific).

Powder X-ray diffraction (XRD) analysis was conducted at the Pacific NorthWest National Laboratory with an automated Bruker D8 diffractometer using of $\text{Cu K}\alpha$ radiation (1.5417 \AA) at a current and voltage of 30 mA and 40 kV, respectively. The XRD patterns were collected from 10° 2θ to 110° 2θ with a step size and dwell time of 0.02° 2θ and 2s, respectively.

Identification of metal(loid) bearing phases using TEM and STEM

The metal(loid)-bearing phases in the OM particles are identified based on a combination of d-spacings observed in selected area diffraction (SAED) pattern and high-resolution TEM (HRTEM) images (in combination with FFT pattern) and semi-quantitative chemical analyses

determined with energy dispersive spectroscopy (EDS) analyses in Scanning TEM mode. In the absence of any structural information (no diffraction spots in SAED pattern or lattice fringes in HRTEM images), phases within OM particles are named based on their chemical composition (e.g. Fe-(hydr)oxide or silicate).

Figures:

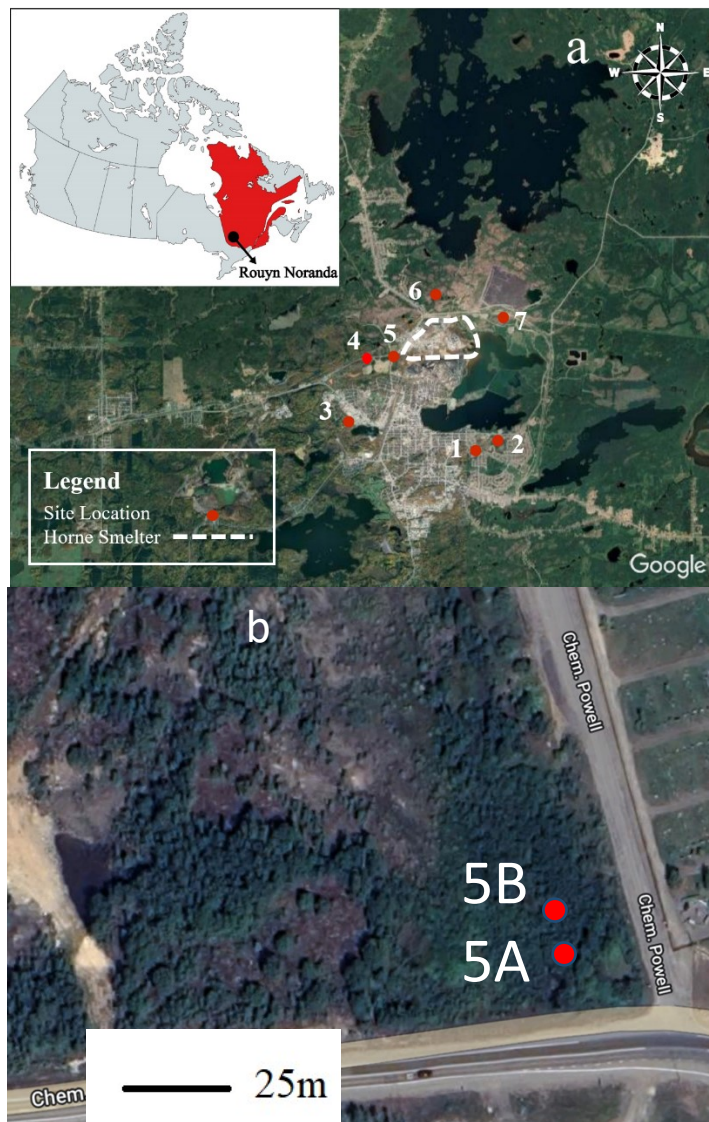


Fig. S1: (a) Map of study area surrounding Horne smelter, red dots represent sampling sites and the Horne Smelter complex is labelled with white dashed line. The inserted image indicates the location of Rouyn Noranda within Quebec, Canada (b) location of the two sampling sites 5A and 5B within a 1250 m² forest area

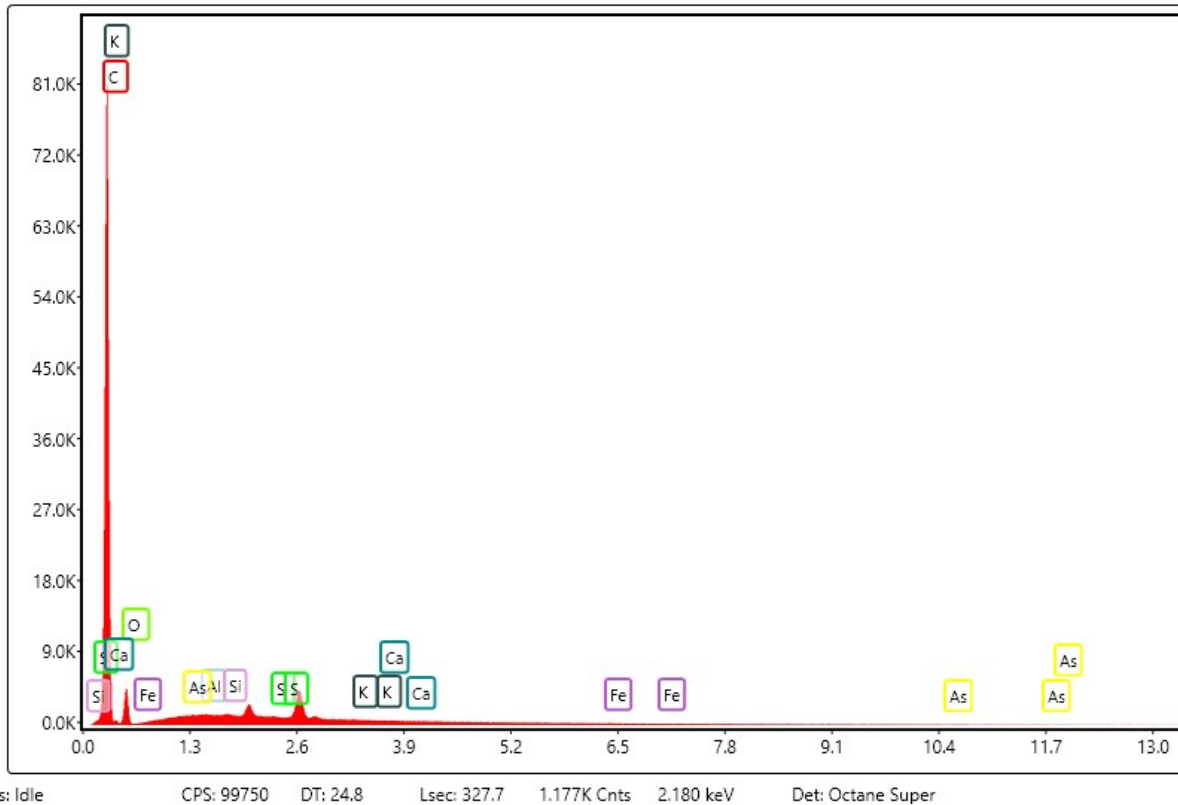


Fig. S2: SEM-EDS of the epoxy indicated traces of S (1% wt) and the absence of any other metal (Loid).

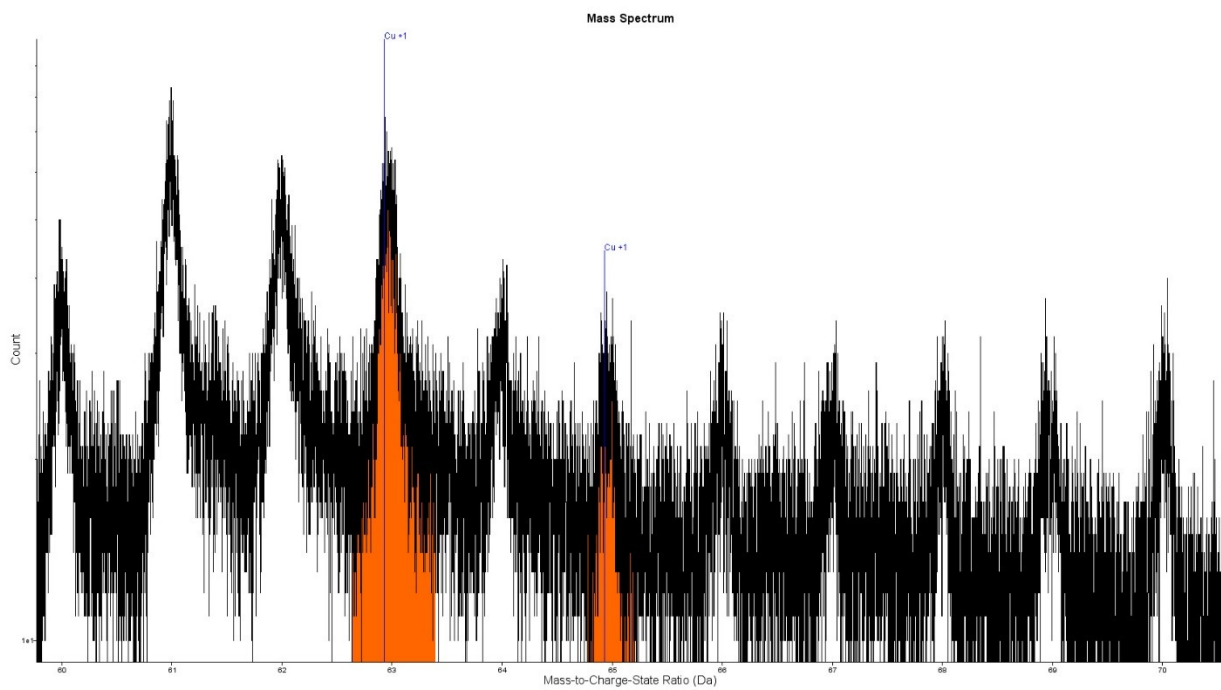


Fig S3: APT mass spectrum for APT-FIB-2: Cu Peaks are color-coded (Orange) and show the relative abundance of Cu^{+1} (63 Da) and Cu^{+1} (65 Da).

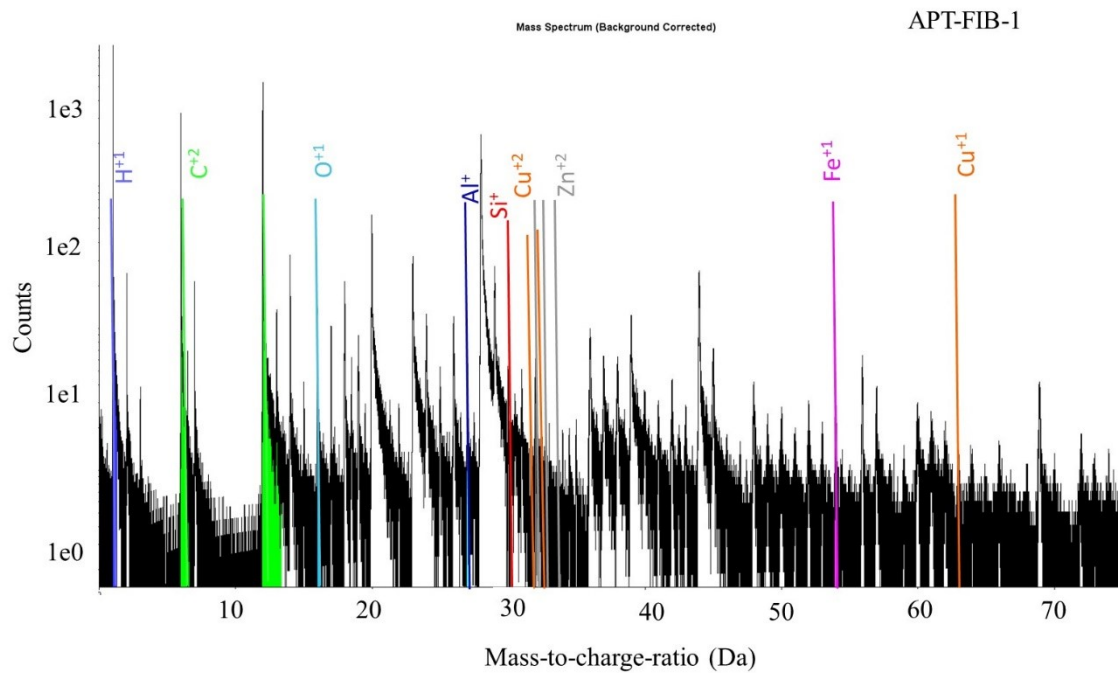


Fig S4: APT mass spectrum for APT-FIB-1: Peaks are color-coded by atomic species showing the positions of H^+ , C^{+2} , O^+ , Al^+ , Si^+ , Cu^{2+} , Cu^+ , Zn^{2+} and Fe^+ . For clarity reasons and due to peak overlap, only a selected number of peaks are labelled.

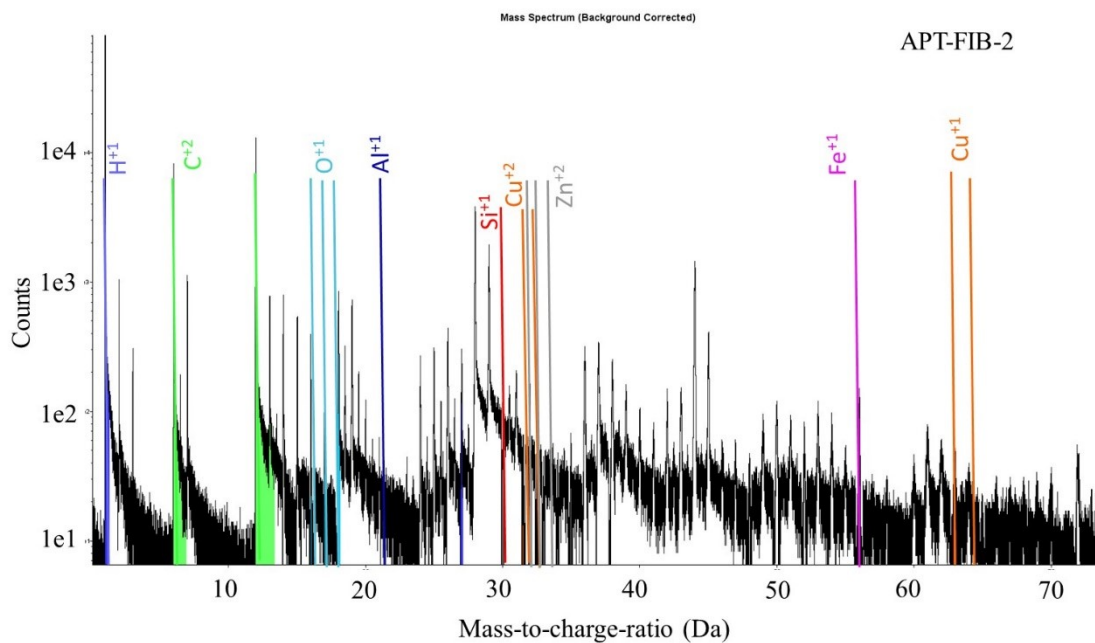


Fig. S5: APT mass spectrum for APT-FIB-2: Peaks are color-coded by atomic species showing the positions of H^+ , C^{+2} , O^{+1} , Al^{+1} , Si^+ , Cu^{+2} , Cu^+ , Zn^{2+} and Fe^+ . For clarity reasons and due to peak overlap, only a selected number of peaks are labelled.

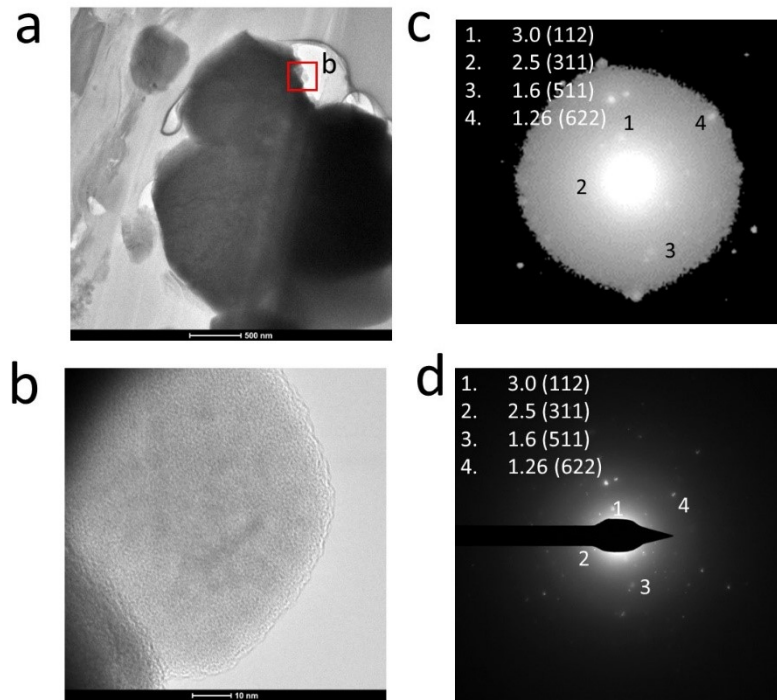


Fig. S6: Supporting data for cuprospinel in Figure 3: (a) TEM image, the area shown in (b) is indicated with a red square; (c) FFT pattern on the area shown in (b); (d) SAED pattern of the area shown in (a).

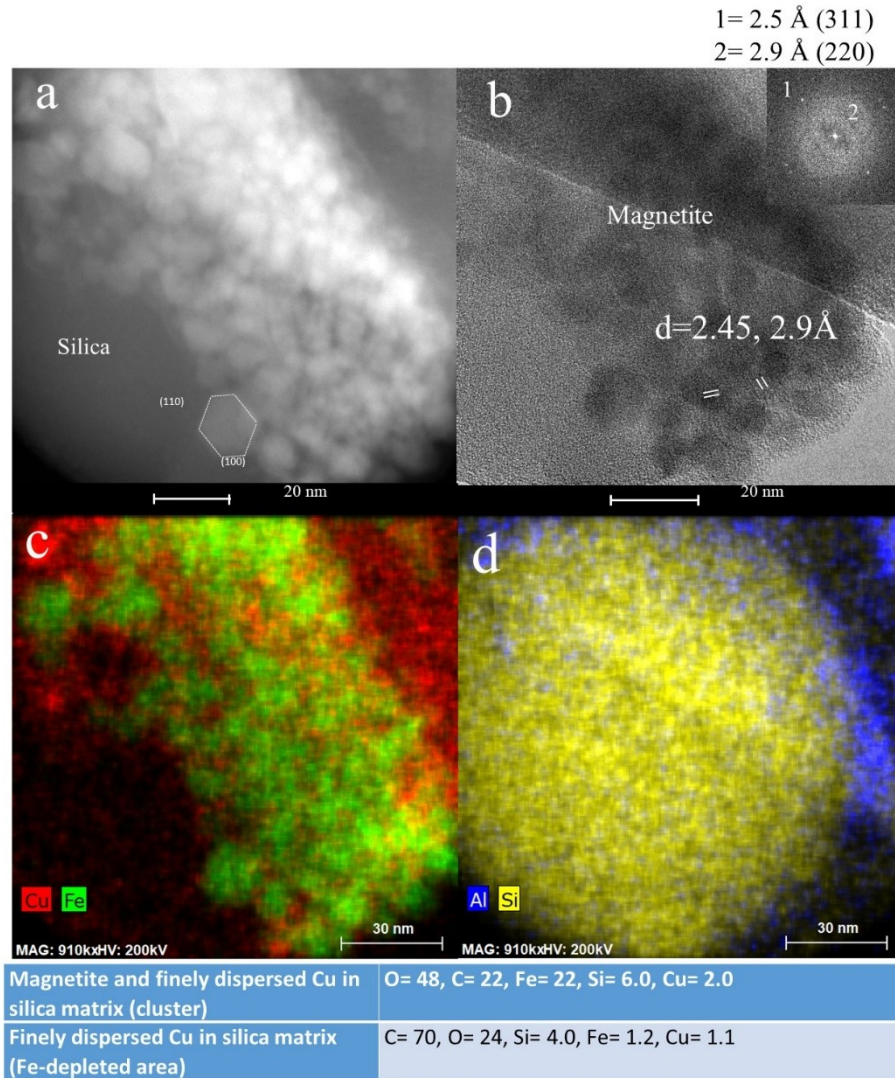


Fig.S7: Another example of the common occurrence of Cu with nanoparticles of magnetite in an amorphous silica inclusion within an OM matrix: (a) STEM image, (b) High resolution TEM image with $d= 2.46 \text{ \AA}$ and 2.91 \AA and (c-d) STEM-EDS chemical distribution map for (c) Cu (red), Fe (green) and (d) Al (blue) and Si (yellow); results of the semi-quantitative analyses of the observed phases are given below the image.

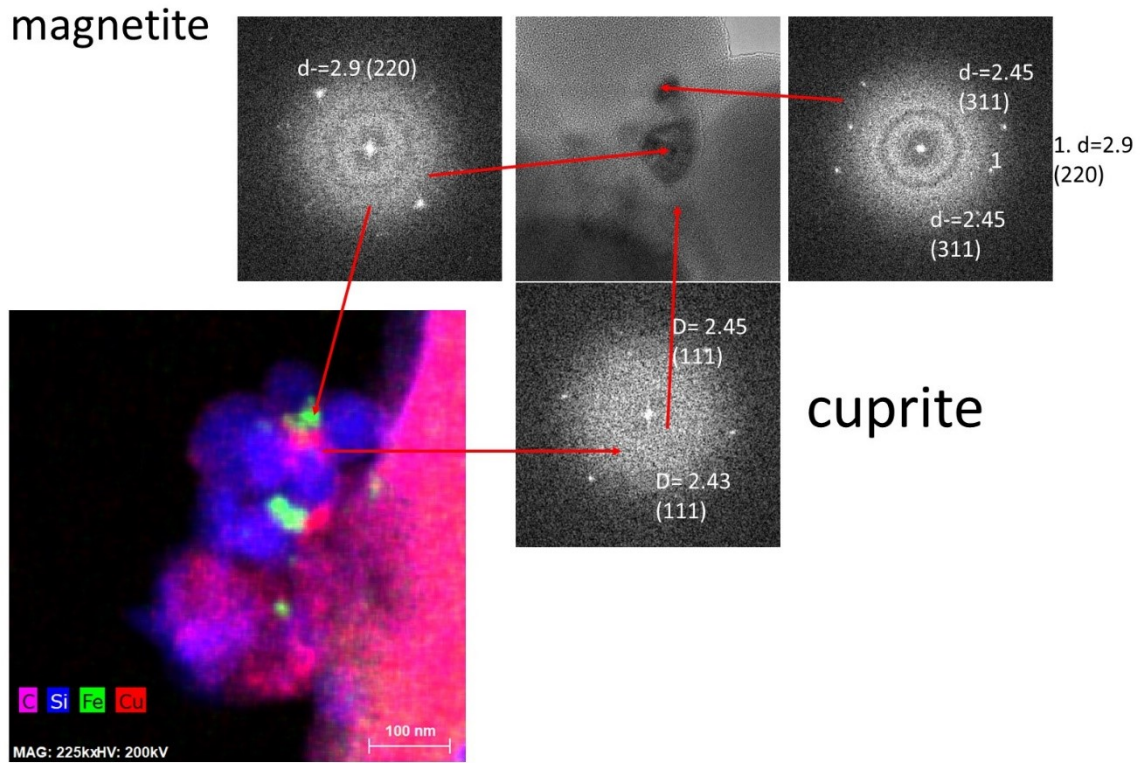


Fig. S8: Supporting data for the occurrence of magnetite and cuprite in the interstices of the silica spheres (Fig. 5): on the top and right: FFT pattern of a magnetite/cuprite inclusion within an interstices between four silica spheres; red arrows indicating the location of the inclusions and FFT pattern with a respect to a STEM-EDS chemical distribution map for C (pink), Si (blue), Fe (green) and Cu (red) (lower left bottom).

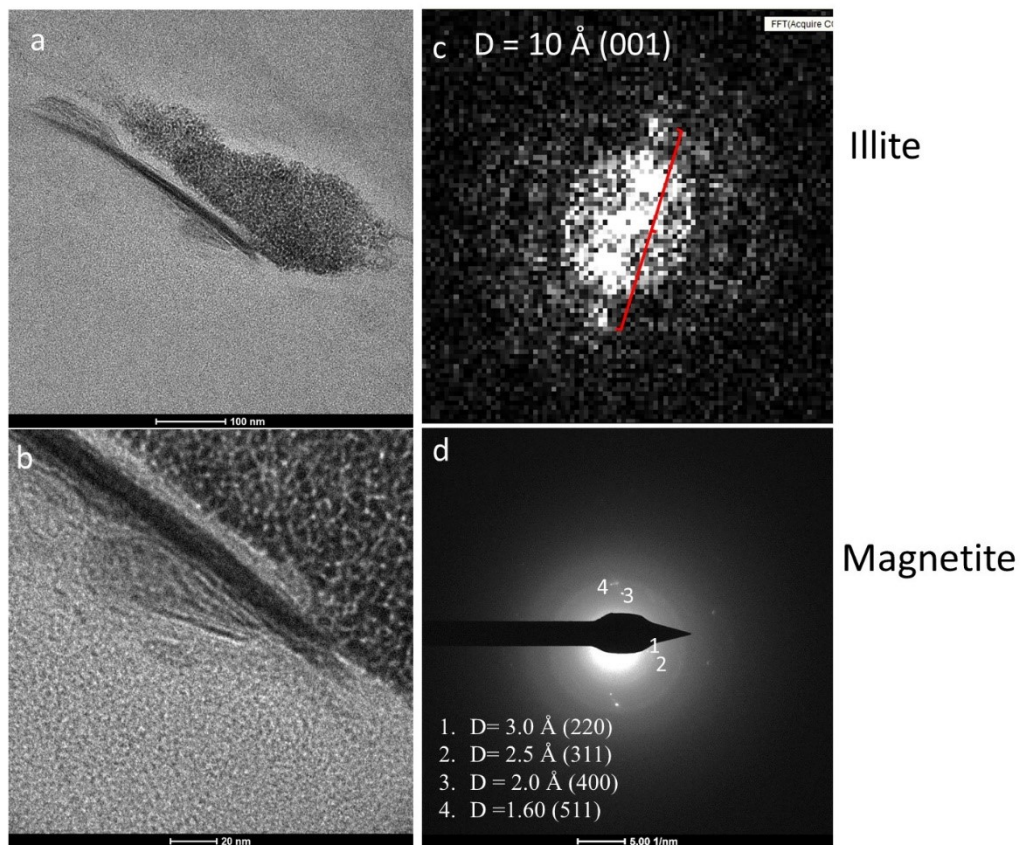


Fig. S9: Supporting data for the common occurrence of an illite lath with a pocket of a cluster of magnetite nanoparticles shown in Figure 6: (a) overview TEM image, (b) underfocused TEM image of illite nano-size domains on the surface of a larger illite lath; (c) FFT pattern of the nano-size illite latches; (d) SAED pattern of the magnetite cluster.

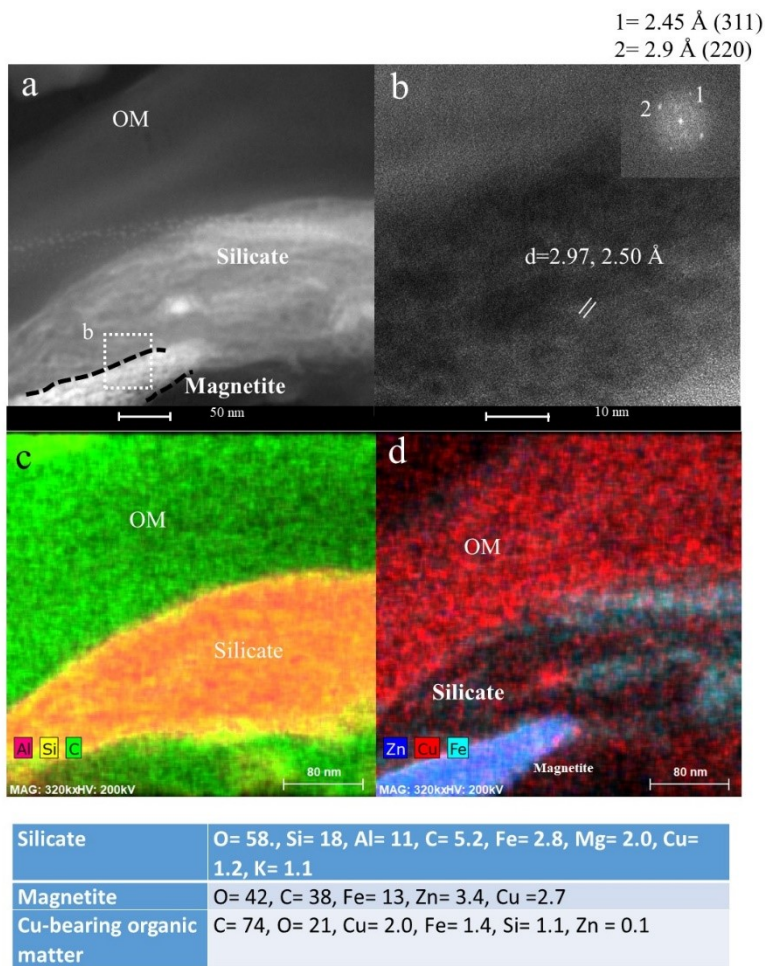


Fig. S10: Additional example for the occurrence of finely dispersed Cu and magnetite within the OM matrix: (a) STEM image, (b) High resolution TEM depicting characteristic lattice fringes of magnetite with $d= 2.97 \text{ \AA}$ and 2.5 \AA and (c-d) STEM-EDS chemical distribution map for (c) Al (red), Si (yellow) and C (green) and (d) Zn (blue), Cu (red) and Fe (light blue); results of semi-quantitative chemical analyses is listed below the image and indicate in combination with the observed s-spacings, the occurrence of a Zn-bearing magnetite, a Cu-bearing silicate phase, and finely dispersed Cu in the OM matrix.

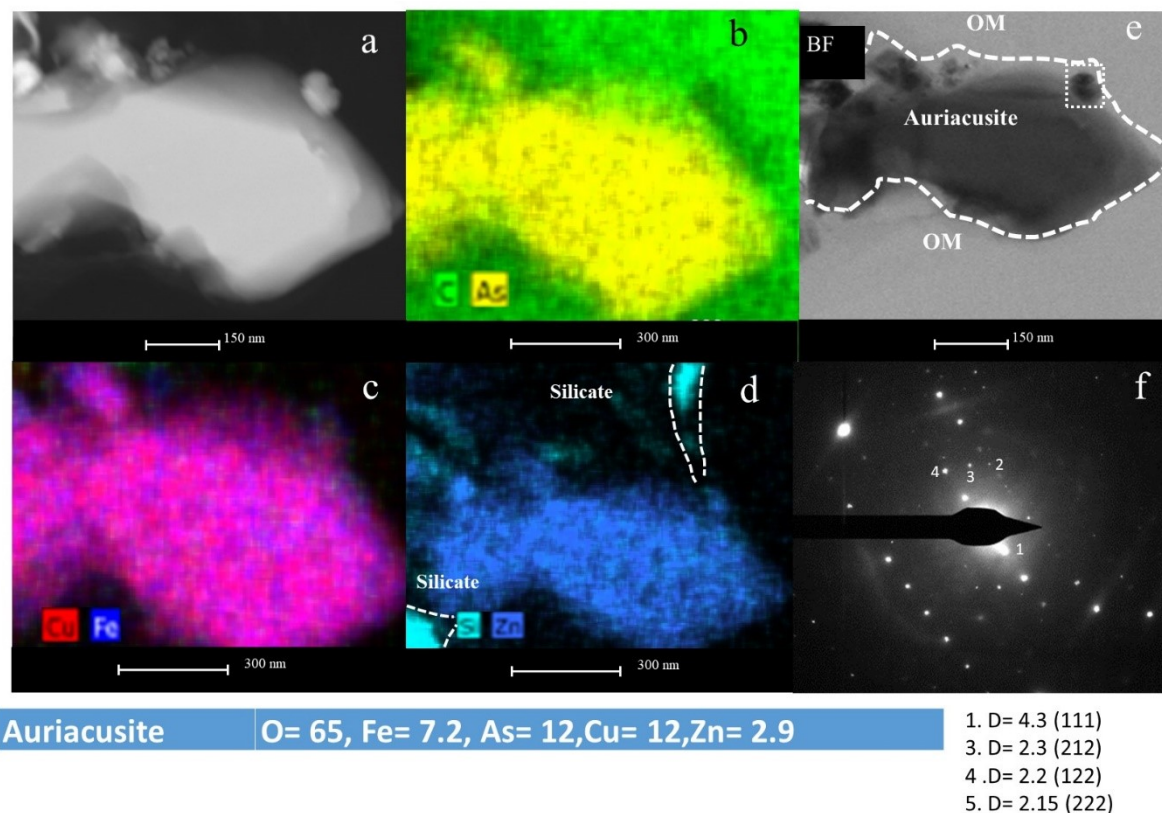


Fig. S11: Example of an oxy-salt mineral in the OM matrix of TEM-FIB2: Auriacusite, a Cu-, Zn-, Fe-bearing arsenate; (a) STEM image, (b)-(d) STEM-EDS chemical distribution maps for (b) C (green) and As (yellow); (c) Cu (red) and Fe (blue) and (d) Si (light blue) and Zn (dark blue); (e) TEM image and (f) SAED pattern; the results of a semi-quantitative chemical analysis and the d-spacing observed in the SAED pattern listed below the image.

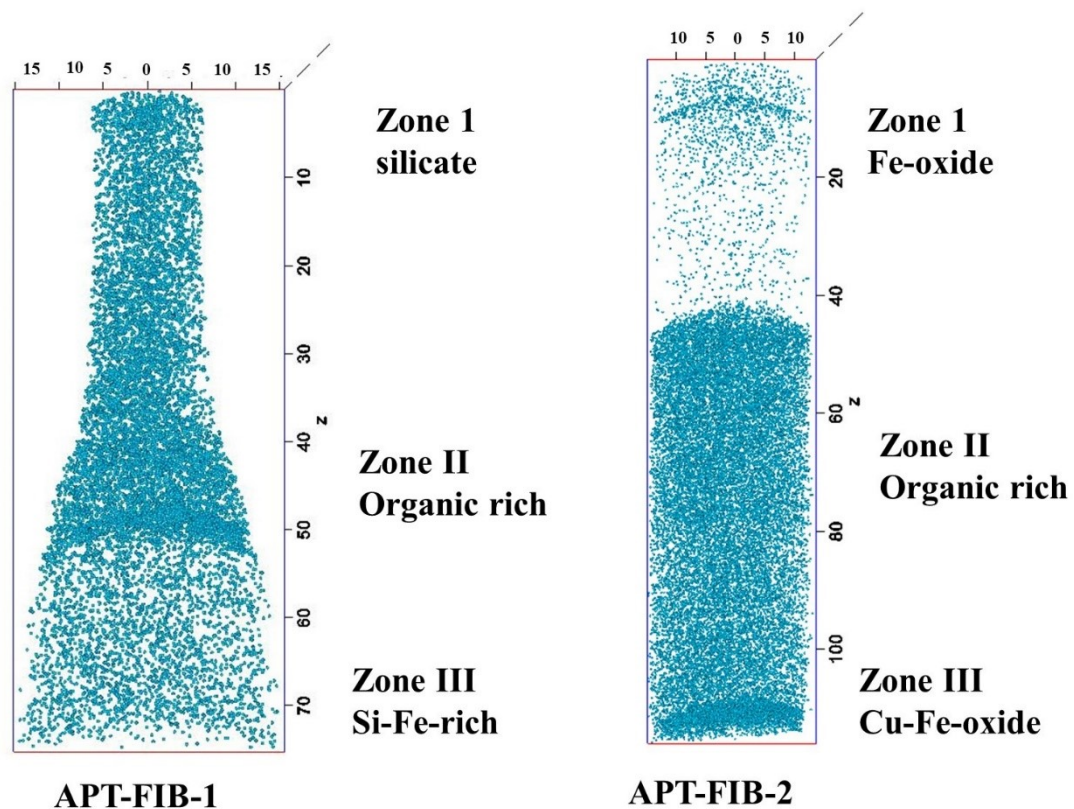


Fig. S12: 3D APT plot indicating the distribution of Oxygen in APT-FIB-1 and APT-FIB-2. The zones identified are labelled accordingly. The lack of Oxygen in zone 1 is most likely due to the occurrence of unidentified O-bearing complex molecules.

References

1. M. Schindler and M. F. Hochella, Sequestration of Pb–Zn–Sb-and As-bearing incidental nanoparticles by mineral surface coatings and mineralized organic matter in soils, *Environmental Science: Processes & Impacts*, 2017, **19**, 1016-1027.
2. V. Ettler, Soil contamination near non-ferrous metal smelters: a review, *Applied Geochemistry*, 2016, **64**, 56-74.
3. S. Lanteigne, M. Schindler, A. M. McDonald, K. Skeries, Y. Abdu, N. M. Mantha, M. Murayama, F. C. Hawthorne and M. F. Hochella, Mineralogy and weathering of smelter-derived spherical particles in soils: implications for the mobility of Ni and Cu in the surficial environment, *Water, Air, & Soil Pollution*, 2012, **223**, 3619-3641.
4. M. Schindler, S. Lanteigne, A. M. McDonald and M. F. Hochella Jr, Evidence of Cu-and Ni-bearing surface precipitates and adsorption complexes in remediated soils at the nanoscale: A TEM, micro-Raman, and laser-ablation ICP-MS study of mineral surface coatings, *The Canadian Mineralogist*, 2016, **54**, 285-309.
5. D. J. Kerr and H. L. Gibson, A comparison of the Horne volcanogenic massive sulfide deposit and intracauldron deposits of the Mine Sequence, Noranda, Quebec, *Economic Geology*, 1993, **88**, 1419-1442.
6. F. T. Denis, An Investigation of the Mineral Composition of the Ores of Noranda Mines Ltd, *McGill University Libraries*, 1933.
7. I. M. Kettles and G. F. Bonham-Carter, Modelling dispersal of metals from a copper smelter at Rouyn-Noranda (Québec, Canada) using peatland data, *Geochemistry: Exploration, Environment, Analysis*, 2002, **2**, 99-110.

8. L. Dinis, C. Bégin, M. M. Savard and M. Parent, Impacts of smelter atmospheric emissions on forest nutrient cycles: Evidence from soils and tree rings, *Science of The Total Environment*, 2020, 141427.
9. C. M. Zdanowicz, C. M. Banic, D. A. Paktunc and D. A. Kliza-Petelle, Metal emissions from a Cu smelter, Rouyn-Noranda, Quebec: characterization of particles sampled in air and snow, *Geochemistry: Exploration, Environment, Analysis*, 2006, **6**, 147-162.
10. R. Knight and P. Henderson, Smelter dust in humus around Rouyn-Noranda, Quebec, *Geochemistry: Exploration, Environment, Analysis*, 2006, **6**, 203-214.
11. G. Bonham-Carter, P. Henderson, D. Kliza and I. Kettles, Comparison of metal distributions in snow, peat, lakes and humus around a Cu smelter in western Quebec, Canada, *Geochemistry: Exploration, Environment, Analysis*, 2006, **6**, 215-228.
12. K. H. Telmer, B. Daneshfar, M. S. Sanborn, D. Kliza-Petelle and D. G. Rancourt, The role of smelter emissions and element remobilization in the sediment chemistry of 99 lakes around the Horne smelter, Quebec, *Geochemistry: Exploration, Environment, Analysis*, 2006, **6**, 187-202.
13. S. Masson, Y. Couillard, P. G. Campbell, C. Olsen, B. Pinel-Alloul and O. Perceval, Responses of two sentinel species (*Hexagenia limbata*—mayfly; *Pyganodon grandis*—bivalve) along spatial cadmium gradients in lakes and rivers in northwestern Québec, *Journal of Environmental Monitoring*, 2010, **12**, 143-158.
14. D. OECD, Guidelines for the testing of chemicals: Leaching in soil columns. *Journal*, 2002.
15. F. Amirault and O. Burnham, Carbon and sulfur analysis in geological samples by combustion-infrared: Verifying method capabilities on new instrumentation, *Summary of Fieldwork and Other Activities 2013, Ontario Geological Survey Open File Report 6290*, 2013, 43-41.
16. O. M. Burnham, Inductively coupled plasma mass spectrometry analysis of trace elements in geological samples after aqua regia extraction at the Geoscience Laboratories: Revised capabilities resulting from new instrumentation, in *Summary of Field Work and Other Activities, Open File Report 6333, Ontario Geological Survey*, 2017, 31.

Table. S1 Trace metal(loid) concentrations in all collected samples around the Horne smelter in Rouyn Noranda. The samples of this study are highlighted.

Sample	Trace metal concentration [mgkg ⁻¹]							Distance to smelter complex [km]
	Ag	Co	Cu	Pb	Sb	Sn	Zn	
1A	18.8	273	2860	1760	28.4	>90	263	3.5
1B	1.4	68.5	854	226	2.2	8.9	118	3.5
1C	19.2	143	4140	909	25.1	72.3	363	3.5
2A	5.1	296	5320	3830	26.1	>90	773	3.1
2B	2.6	154	789	378	4.8	21.5	83	3.1
2C	9.6	81.3	6120	2100	12.5	57.0	707	3.1
3A	8.8	125	2040	2170	13.7	>90	420	2.9
3B	2.7	123	1010	719	4.7	25.3	255	2.9
3C	1.4	275	523	176	2.1	7.9	516	2.9
4A	9.2	105	2850	602	12.9	29.1	656	2.9
4B	11.3	84.6	3420	836	14.6	36.1	507	2.9
4C	0.5	81.4	131	52.0	1.4	3.3	169	2.9
5A	21.9	174	7970	3100	32.9	>90	1470	1.8
5B	23.4	115	6920	1690	35.4	64.5	1520	1.8
6A	8.1	117	3420	495	10.1	24.8	615	1.2
6B	6.4	81.8	1740	927	15.6	32.4	246	1.2
6C	19.8	118	6540	1460	18.3	44.4	692	1.2
6F	12.8	99.2	3730	609	26.7	32.1	1150	1.2
7A	7.4	184	2690	1260	49.0	>90	4230	1.8
7B	7.3	88.0	3830	2023.9	42.6	>90	2178	1.8
7C	5.3	118	1900	875.1	38.9	>90	1480	1.8
Average	10	138	3276	1248	20	33	887	

Table. S2 Carbon-Nitrogen-Sulfur concentrations in the two samples.

Sample	Wt% N	Wt% TC	Wt% S	Wt%TOC	C/N
5A	1.67	28.1	0.28	25.1	16.8
5B	1.54	26.3	0.26	24.6	17.1

